Supporting Information

For

Ligand sphere conversions in terminal carbide complexes

Thorbjørn J. Morsing, Anders Reinholdt, Stephan P. A. Sauer, and Jesper Bendix*

Department of Chemistry, University of Copenhagen, Universitetsparken 5, DK-2100, Denmark

Telephone: +45 35320101; Email: bendix@kiku.dk

Contents

Materials and methods

Syntheses: Unless otherwise stated, no attempts were made to exclude air in the syntheses. Chloroform (Sigma-Aldrich, HPLC, ≥99.8%), chloroform-*d* (Sigma-Aldrich, 99.8% D), dichloromethane (Sigma-Aldrich, HPLC, ≥99.8%), dichloromethane-*d*2 (Sigma-Aldrich, 99.9% D), benzene-*d*6 (Sigma-Aldrich, 99.6% D), Acetonitrile (Riedel-de Haën, >99.9%), diethyl ether (VWR Chemicals), tetraethylammonium fluoride hydrate (Sigma-Aldrich, 98%) and Silica Gel 60 Å (ROCC) were bought from commercial suppliers and used as received. $[Ru(C)Cl_2(PCy_3)_2]$ (**RuC**) and TlOTf were synthesized according to published procedures (Johnson[1], Marks[2]); **Ru^{13}C** was obtained with $^{13}CH_2{}^{13}CHOAc$ (Sigma-Aldrich, 99% ^{13}C). $(Ph_4P)CN$ was prepared by aqueous metathesis of sodium cyanide and tetraphenylphosphonium chloride and recrystallized from water.

Physical measurements

NMR-spectroscopy: ^{1}H-NMR and $^{31}P\{^1H\}$-NMR spectra were recorded on a 500 MHz Bruker instrument with a broad-band probe. ^{19}F-NMR spectra were recorded on a 300 MHz Varian instrument. $^{13}C\{^1H\}$-NMR spectra were recorded on a 500 MHz Bruker instrument with a cryoprobe. For ^{1}H and ^{13}C, residual solvent signals were used for calibration ($CDCl_3$: δ = 7.26 and 77.16 ppm, CD_2Cl_2: δ = 5.33 and 54.24 ppm, C_6D_6: 7.16 and 128.06 ppm for ^{1}H and ^{13}C, respectively). For ^{31}P and ^{19}F, the signals were referenced to the deuterium resonances arising from the solvents. Examples of NMR spectra for selected compounds are shown in Figures S5-S10.

Mass spectrometric measurements were carried out on a Bruker Solarix XR ESI/MALDI FT-ICR MS instrument (ESI, acetonitrile containing formic acid as solvent).

Elemental analyses were performed by the microanalytical services of the Department of Chemistry, University of Copenhagen.

X-ray crystallographic studies: single crystals of all complexes were coated with mineral oil, picked up with nylon loops, and mounted immediately in the nitrogen cold stream of the diffractometer to prevent solvent loss.

Single-crystal X-ray diffraction studies were performed at 122(2) K on a Bruker D8 VENTURE diffractometer equipped with a Mo K_α high-brilliance IμS radiation source (λ = 0.71073 Å), a

multilayer X-ray mirror and a PHOTON 100 CMOS detector, and an Oxford Cryosystems low temperature device. The instrument was controlled with the APEX2 software package using SAINT.[3] Final cell constants were obtained from least squares fits of several thousand strong reflections. Intensity data were corrected for absorption using intensities of redundant reflections with the program SADABS.[4] The structures were solved in Olex2 using the olex2.solve[5] structure solution program (Charge Flipping) and refined using the olex2.refine program[6] or SHELXL.[7] All non-hydrogen atoms were refined anisotropically and hydrogen atoms were placed at calculated positions and refined as riding atoms with isotropic displacement parameters (U_{iso} = 1.2 U_{eq} of the parent atom, except for methyl hydrogens which were constrained to 1.5 U_{eq} of the parent atom).

Disorder in solvent molecules and counterions was treated with appropriate choices of the EADP, ISOR, and SADI commands. For the neutral **RuC-X** structures, the X and chloride ligands are disordered over the two ligand positions. This makes the bond metrics for these ligands less well determined. CCDC numbers 1417880-1417885 contain the crystallographic data reported herein. These data can be obtained free of charge from The Cambridge Crystallographic Data Centre via www.ccdc.cam.ac.uk/data_request/cif. Selected crystallographic figures (Figure S1) and details (Table S1) are below.

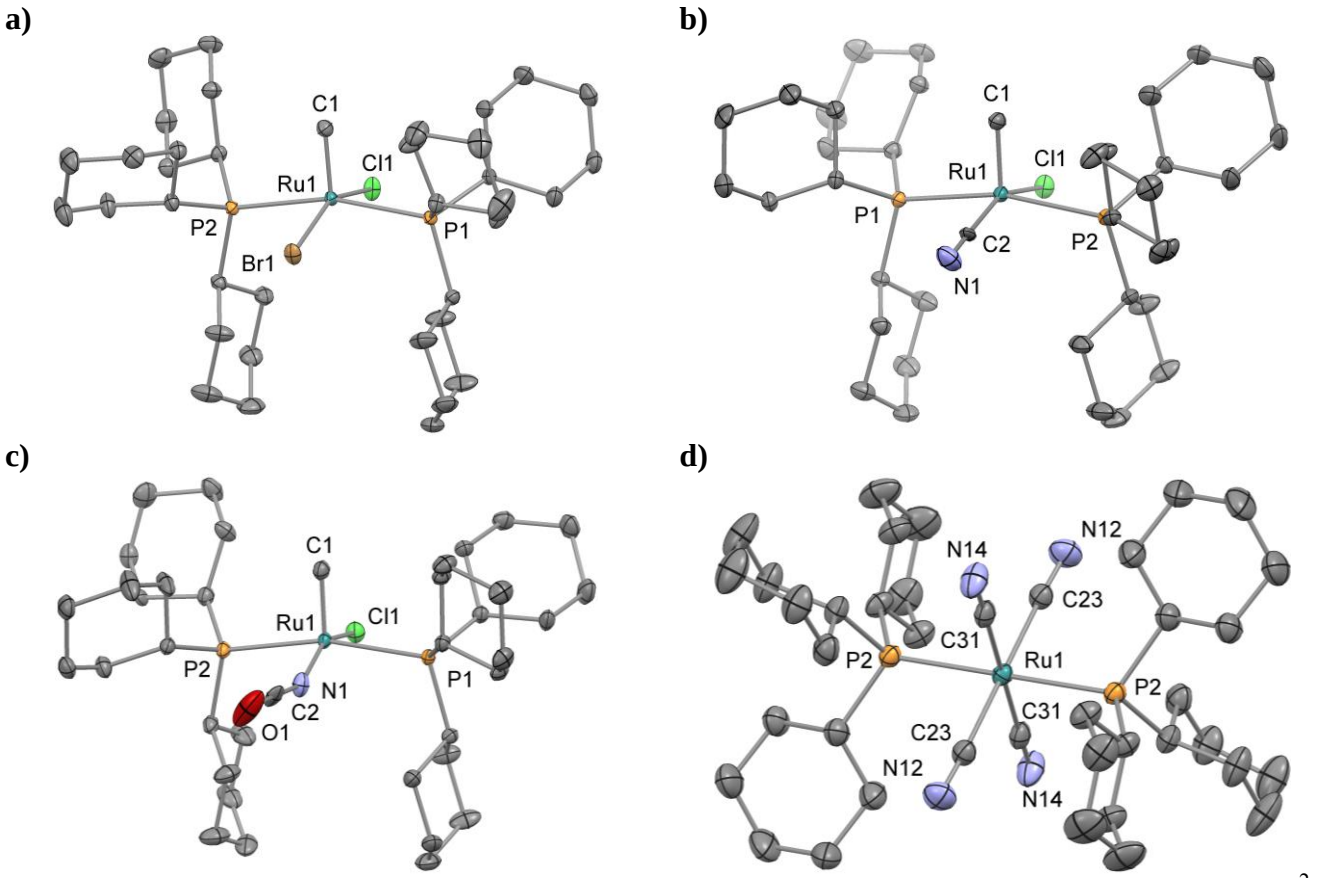

Figure S1 Molecular structures of **RuC-Br**, **RuC-CN**, **RuC-NCO** and $[Ru(PCy_3)_2(CN)_4]^{2-}$. Displacement ellipsoids correspond to 50%. H-atoms, co-crystallised chloroform, and PPh_4^+ are omitted.

Table S1. Crystallographic data

Compound	**RuC–$(CN)_2$** (CCDC 1417881)	**RuC–MeCN** (CCDC 1417884)	**RuC–Br** (CCDC 1417882)
Empirical formula	$C_{39}H_{66}N_2P_2Ru$	$C_{40}H_{69}ClF_3NO_3P_2RuS$	$C_{37}H_{66}BrClP_2Ru$
Formula weight	725.95	899.48	789.26
Temperature / K	122(2)	122(2)	122(2)
Crystal system	monoclinic	triclinic	monoclinic
Space group	$P2_1/c$	$P\bar{1}$	$P2_1/n$
a / Å	13.9870(8)	10.0150(16)	13.2074(5)
b / Å	14.9950(9)	14.317(2)	23.3788(9)
c / Å	20.2280(11)	15.830(2)	13.6727(5)
α / °	90.00	81.185(6)	90
β / °	112.449(2)	86.493(6)	115.7250(10)
γ / °	90.00	72.928(6)	90
V / Å^3	3921.0(4)	2143.9(6)	3803.3(2)
Z	4	2	4
ρ_{calc} / g cm^{-3}	1.230	1.393	1.378
μ / mm^{-1}	0.509	0.601	1.641
2θ range / °	4.16 to 50.7	4.446 to 54.206	4.804 to 53.464
Reflections collected	139492	106298	58146
Independent reflections	7172 [R_{int} = 0.0947]	9456 [R_{int} = 0.0661]	8071 [R_{int} = 0.0571]
Restraints / parameters	0 / 397	0 / 470	2 / 398
Goodness-of-fit on F^2	1.071	1.033	1.020
Final R indexes [$I>=2\sigma(I)$]	R_1 = 0.0338, wR_2 = 0.0818	R_1 = 0.0276, wR_2 = 0.0651	R_1 = 0.0266, wR_2 = 0.0509
Final R indexes [all data]	R_1 = 0.0506, wR_2 = 0.0917	R_1 = 0.0328, wR_2 = 0.0678	R_1 = 0.0384, wR_2 = 0.0543
Largest diff. peak/hole / e Å^{-3}	2.21 / –0.35	0.64 / –0.64	0.45 / –0.53

Compound	**RuC-(CN)** (CCDC 1417883)	**RuC-NCO** (CCDC 1417885)	$[Ru(PCy_3)_2(CN)_4]^{2-}$ (CCDC 1417880)
Empirical formula	$C_{38}H_{66}ClNP_2Ru$	$C_{38}H_{66}ClNOP_2Ru$	$C_{94}H_{112}Cl_{18}N_4P_4Ru$
Formula weight	735.37	751.37	2160.92
Temperature / K	122(2)	122(2)	122(2)
Crystal system	monoclinic	monoclinic	triclinic
Space group	$P2_1/n$	$P2_1/n$	$P\bar{1}$
a / Å	13.2252(6)	13.1947(4)	12.421(4)
b / Å	23.4044(10)	23.4389(7)	13.919(4)
c / Å	13.5975(7)	13.5623(4)	16.511(6)
α / °	90	90	88.966(15)
β / °	115.829(2)	115.4970(10)	76.208(15)
γ / °	90	90	67.398(14)
V / Å^3	3788.3(3)	3785.9(2)	2550.8(15)
Z	4	4	1
ρ_{calc} / g cm^{-3}	1.289	1.318	1.407
μ / mm^{-1}	0.595	0.599	0.734
2θ range / °	4.998 to 53.466	4.812 to 51.362	4.192 to 54.204
Reflections collected	20514	55196	110335
Independent reflections	7981 [R_{int} = 0.0500]	7186 [R_{int} = 0.0520]	11246 [R_{int} = 0.0683]
Restraints / parameters	12 / 416	7 / 461	0 / 630
Goodness-of-fit on F^2	1.035	1.067	1.068
Final R indexes [$I>=2\sigma(I)$]	R_1 = 0.0425, wR_2 = 0.0976	R_1 = 0.0293, wR_2 = 0.0632	R_1 = 0.0654, wR_2 = 0.1670
Final R indexes [all data]	R_1 = 0.0572, wR_2 = 0.1035	R_1 = 0.0384, wR_2 = 0.0665	R_1 = 0.0801, wR_2 = 0.1826
Largest diff. peak/hole / e Å^{-3}	0.83 / –0.71	0.50 / –0.37	1.35 / –1.18

Computational details

Calculations were performed on model compounds where the large cyclohexyl groups of the experimental carbide complexes has been exchanged for methyl groups to greatly ease the computational burden.

All geometries were optimised in the ORCA programme[8] using density functional theory with the PBE0 exchange-correlation functional[9] and the Ahlrichs VTZ(2df) basis set[10]. Relativistic effects were taken into account with the spin-orbit ZORA approximation[11] the effect of the solvent was modelled with the COSMO screening model[12] (using parameters for dichloromethane). The spin-orbit ZORA calculations of scaled nuclear magnetic shieldings and spin-spin coupling constants were carried out with the ADF program[13] at the density functional theory level with the PBE0 exchange-correlation functional, the QZ4P basis set[14] and a spherical Gaussian nuclear charge distribution model.

Table S2. Calculated nuclear magnetic shieldings and chemical shifts[a)]

Compound	Carbide nuclear magnetic shielding (in ppm)				Carbide chemical shift (in ppm)			
	σ_{para}^{ZORA}	σ_{dia}^{ZORA}	σ_{SO}^{ZORA}	σ^{ZORA}	σ_{para}^{ZORA}	σ_{dia}^{ZORA}	σ_{SO}^{ZORA}	σ^{ZORA}
$[RuC(P(CH_3)_3)_2Cl_2]$	-549.51	263.57	2.22	-283.73	484.70	-13.78	-1.40	469.52
$[RuC(P(CH_3)_3)_2(CN)_2]$	-567.23	284.74	1.48	-281.00	502.42	-34.95	-0.67	466.79
$[RuC(P(CH_3)_3)_2ClF]$	-553.23	262.90	2.06	-288.28	488.42	-13.11	-1.24	474.07
$[RuC(P(CH_3)_3)_2ClBr]$	-544.78	262.92	1.69	-280.16	479.97	-13.14	-0.88	465.95
$[RuC(P(CH_3)_3)_2ClI]$	-540.41	262.63	0.32	-277.46	475.60	-12.85	0.50	463.26
$[RuC(P(CH_3)_3)_2Cl(CN)]$	-553.22	260.99	2.06	-290.16	488.41	-11.21	-1.25	475.96
$[RuC(P(CH_3)_3)_2Cl(\underline{N}CO)]$	-557.82	261.65	1.71	-294.46	493.02	-11.86	-0.90	480.25
$[RuC(P(CH_3)_3)_2Cl(\underline{O}CN)]$	-563.36	262.11	1.86	-299.38	498.56	-12.33	-1.05	485.18
$[RuC(P(CH_3)_3)_2Cl(\underline{N}CS)]$	-561.30	261.68	1.77	-297.86	496.49	-11.89	-0.95	483.65
$[RuC(P(CH_3)_3)_2Cl(NCCH_3)]^+$	-568.35	260.10	1.46	-306.79	503.54	-10.31	-0.65	492.58

[a)] relative to the calculated carbon magnetic shielding in TMS: σ_{para}^{ZORA}=-64.81 ppm, σ_{dia}^{ZORA}=249.79 ppm, σ_{SO}^{ZORA}=0.81 ppm, σ^{ZORA}=185.79 ppm.

Table S3 Calculations were made on **RuC** with **RuC-(CN)$_2$** ligand angles (**RuC***) and **RuC-(CN)$_2$** with **RuC** ligand angles (**RuC-(CN)$_2$***) and the calculted shieldings are here compared to **RuC** and **RuC-(CN)$_2$**.

Geometry	$\Delta\sigma_{para}^{ZORA}$ /ppm	$\Delta\sigma_{dia}^{ZORA}$ /ppm	$\Delta\sigma_{SO}^{ZORA}$ /ppm	$\Delta\sigma^{ZORA}$ /ppm
RuC* compared to **RuC**	-21.94	-0.93	-0.92	-23.80
(**RuC-(CN)$_2$*** compared to (**RuC-(CN)$_2$**	51.39	-24.94	0.25	26.70
RuC* compared to (**RuC-(CN)$_2$**	33.67	-3.77	-0.48	29.42
(**RuC-(CN)$_2$*** compared to **RuC**	-4.22	-22.10	-0.19	-26.52

Kinetic studies

When **RuC** reacts with cyanide, the cyclohexyl ^{1}H-NMR resonances conveniently change sufficiently to deduce the reaction order and the reaction rate. It is seen in Figure S2 that three PCy_3-species are dominant in the reaction mixture. This is interpreted in terms of the simplified reaction scheme:

RuC → **RuC-(CN)$_2$** → $[Ru(PCy_3)_2(CN)_4]^{2-}$

In the first step, **RuC** transforms to **RuC-(CN)$_2$** (rate constant k_1). **RuC-CN** is not observed, suggesting the probable intermediate to react rapidly with cyanide compared with **RuC**. In the second step, **RuC-(CN)$_2$** decomposes to $[Ru(PCy_3)_2(CN)_4]^{2-}$ (rate constant k_2). The reactions were carried out in chloroform under pseudo steady-state conditions (>20-fold excess of cyanide) at five cyanide concentrations. By fitting the time-evolution of the **RuC** and **RuC-(CN)$_2$** integrals to the expressions below, pseudo first order rate constants, k_1' and k_2' were determined in six δ_H intervals for each experiment:

$$[\mathbf{RuC}] = [\mathbf{RuC}]_0 \times e^{-k_1' t}$$

$$[\mathbf{RuC\text{-}(CN)_2}] = [\mathbf{RuC}]_0 \frac{k_1'}{k_2' - k_1'} \left(e^{-k_1' t} - e^{-k_2' t} \right)$$

Representative fits are given in Figure S3. Plots of averaged k_1' against $[CN^-]$ describe a straight line, suggesting a first order reaction in cyanide and thus a second order reaction in total (Figure S4). The slope yields the true second order rate constant, k_1 = 0.0104(6) s^{-1} M^{-1}. The second reaction is slow, resulting in a large variance of the thus ill-defined k_2.

Supporting figures

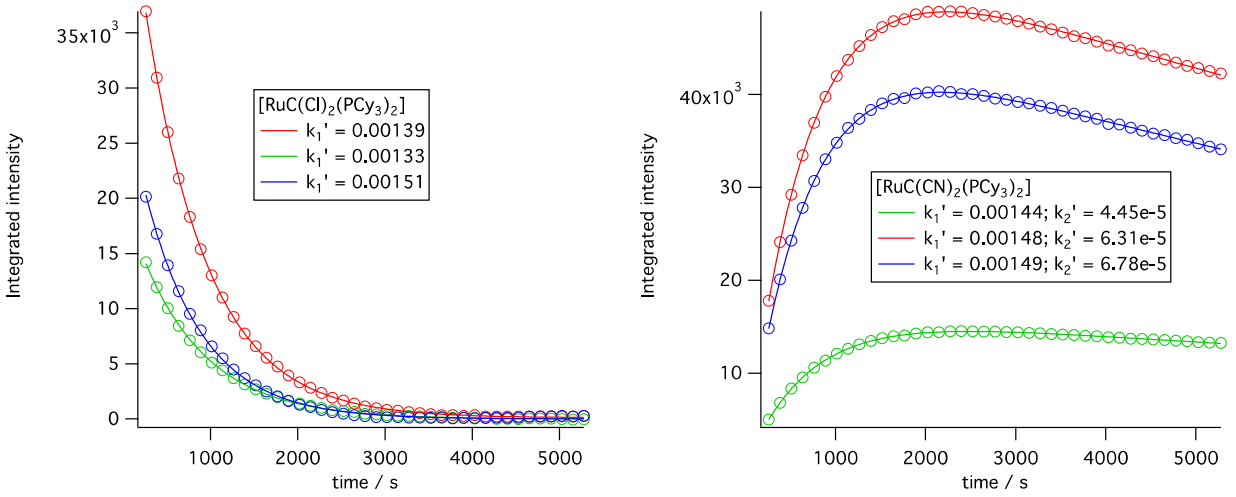

Figure S2 Integral graphs for **RuC** and **RuC-(CN)$_2$** for one steady state kinetics experiment. The averaged k_1' obtained from this run at [CN^-] = 0.160 M is 0.00144(7) s^{-1}.

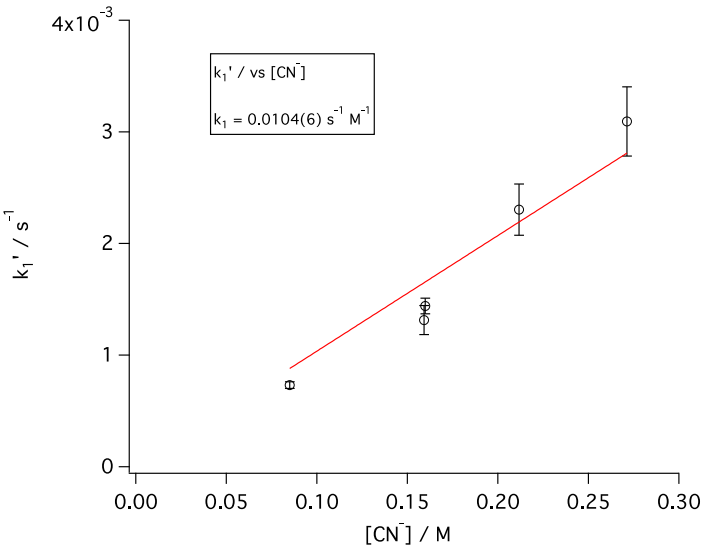

Figure S3 k_1' plotted against the cyanide concentration gives the true second order rate constant, k_1, as the slope. The line has been forced through the origin.

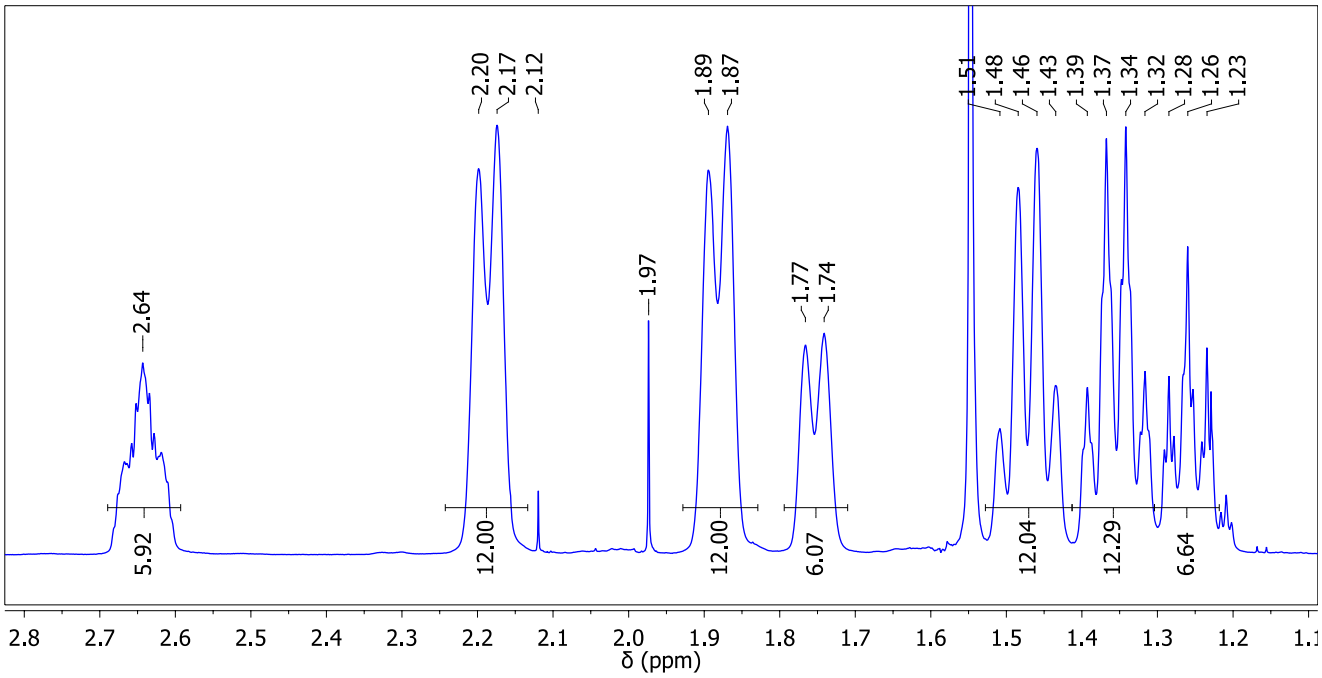

Figure S4 The PCy_3 region of the ^{1}H-NMR spectrum of **RuC-(CN)$_2$** measured in CD_2Cl_2. The resonances at 1.97 and 1.52 ppm arise from traces of acetonitrile and water.

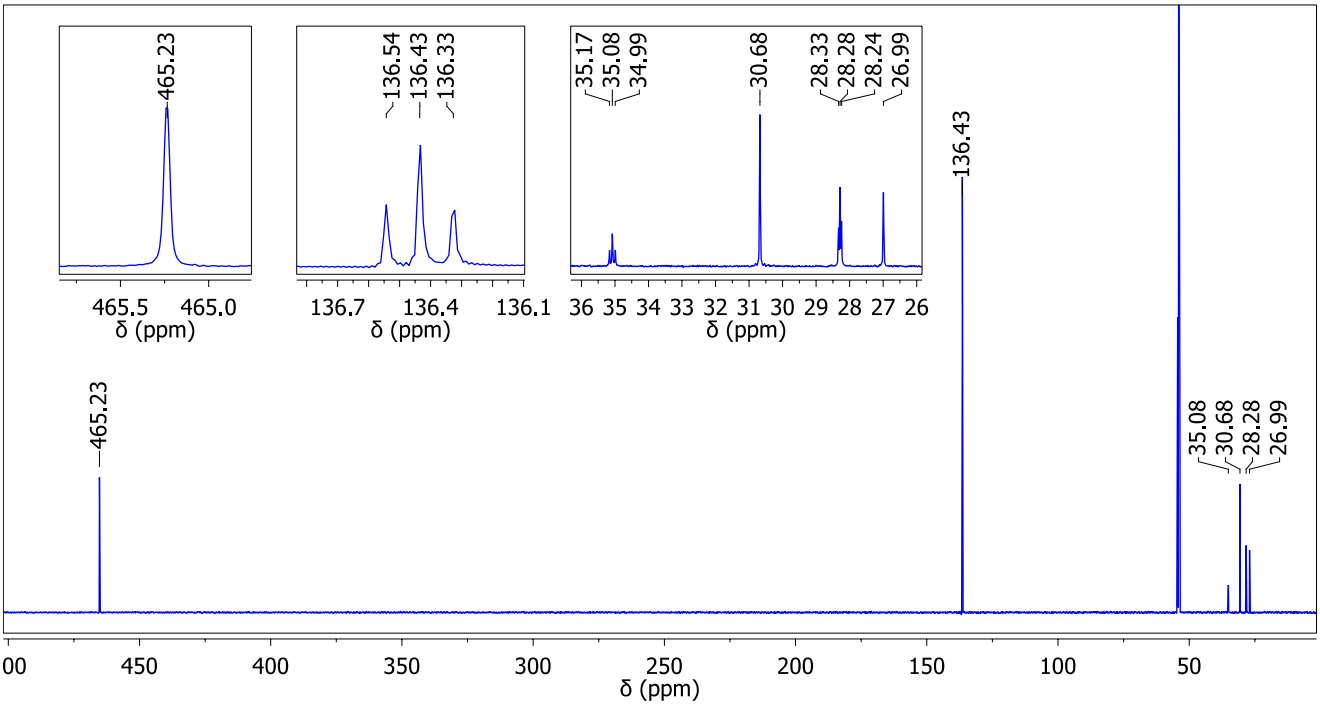

Figure S5 ^{13}C-NMR spectrum of **RuC-(CN)$_2$** measured in CD_2Cl_2.

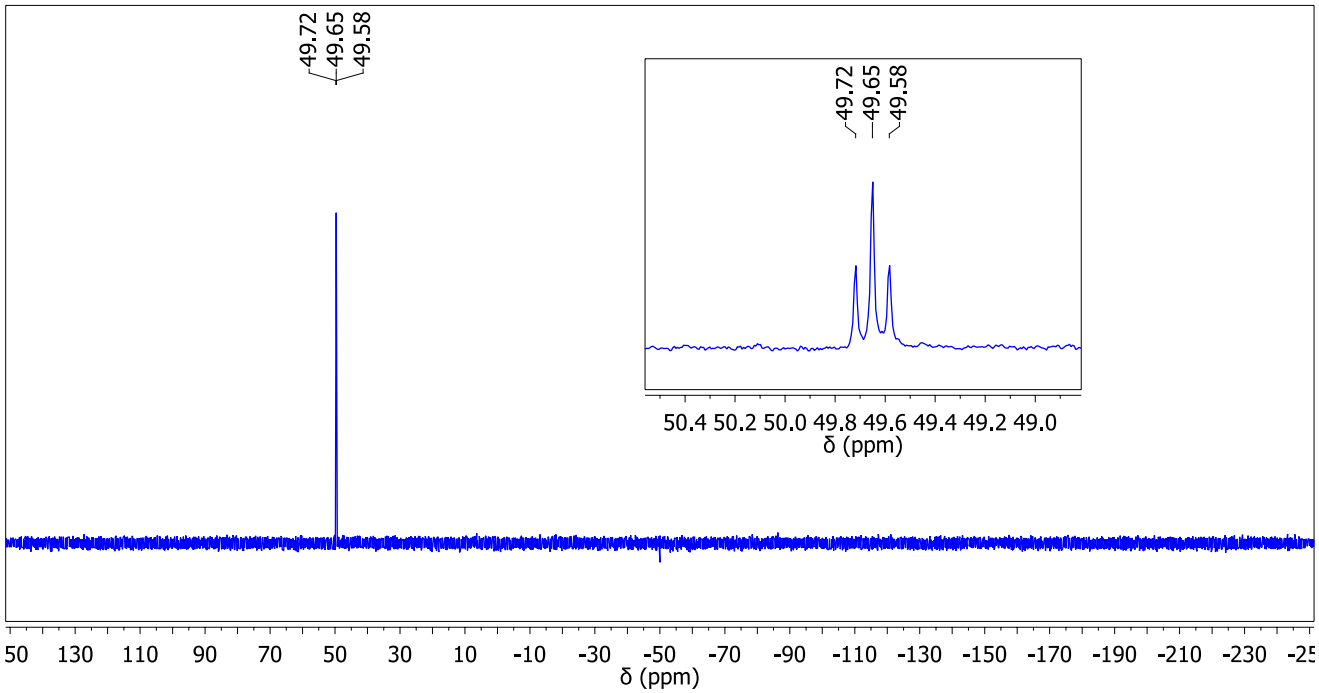

Figure S6 ^{31}P-NMR spectrum of **RuC-(CN)$_2$** measured in CD_2Cl_2.

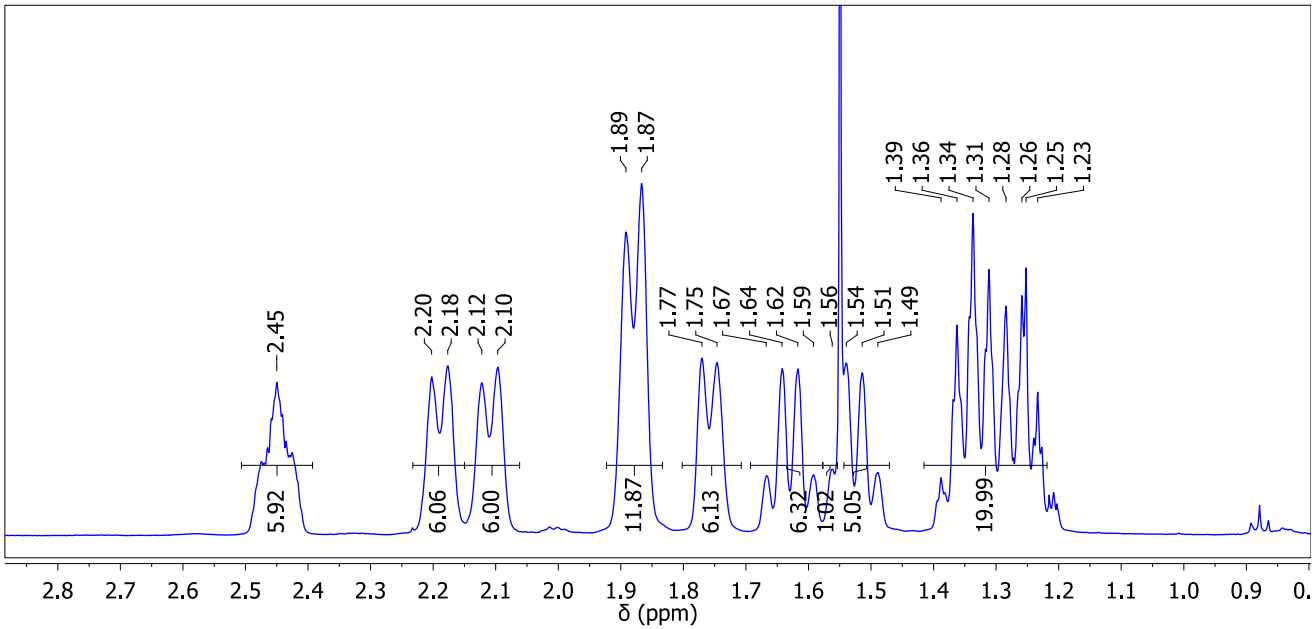

Figure S7 The PCy_3 region of the ^{1}H-NMR spectrum of **RuC-NCS** measured in $CDCl_3$. The resonance at 1.56 stems from a trace of water in the solvent.

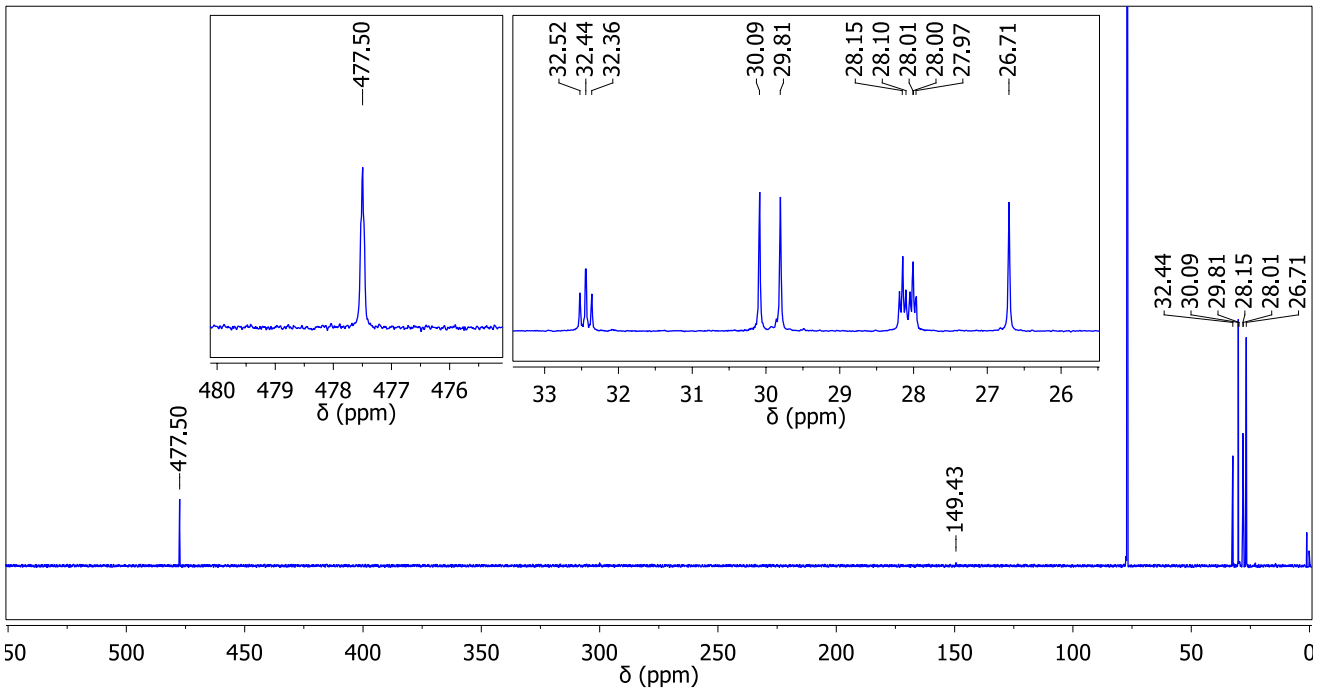

Figure S8 ^{13}C-NMR spectrum of **RuC-NCS** measured in $CDCl_3$.

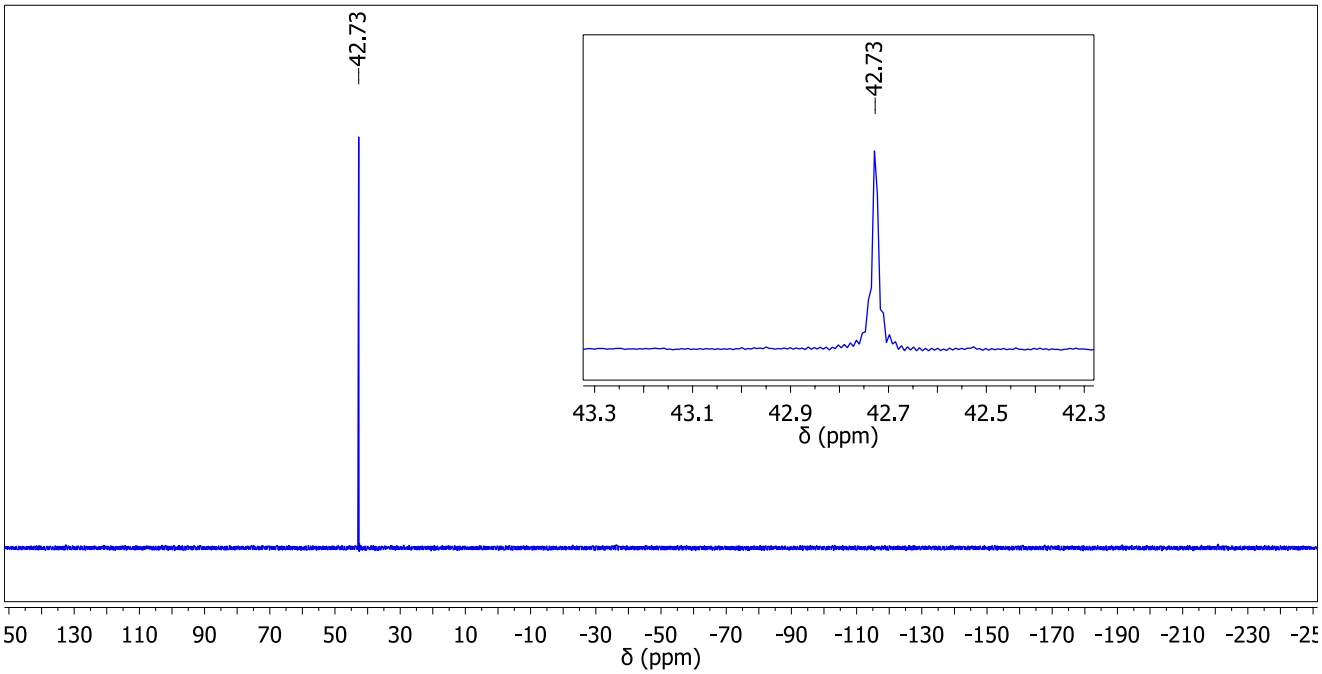

Figure S9 ^{31}P-NMR spectrum of **RuC-NCS** measured in $CDCl_3$.

References

1. Caskey, S. R.; Stewart, M. H.; Kivela, J. E.; Sootsman, J. R.; Johnson, M. J. A.; Kampf, J. W., *J. Am. Chem. Soc.* **2005,** *127*, 16750-16751.
2. Woodhouse, M. E.; Lewis, F. D.; Marks, T. J., *J. Am. Chem. Soc.* **1982,** *104*, 5586-5594.
3. *Bruker; Bruker AXS, Inc. SAINT, Version 7.68A; Bruker AXS: Madison, WI, 2009.*
4. Sheldrick, G., *SADABS, Version 2008/2; University of Göttingen: Germany, 2003.*
5. Dolomanov, O. V.; Bourhis, L. J.; Gildea, R. J.; Howard, J. A. K.; Puschmann, H., *J. Appl. Crystallogr.* **2009,** *42*, 339-341.
6. Bourhis, L. J.; Dolomanov, O. V.; Gildea, R. J.; Howard, J. A. K.; Puschmann, H., *Acta Crystallogr., Sect. A* **2015,** *71*, 59-75.
7. Sheldrick, G., *Acta Crystallogr., Sect. A* **2008,** *64*, 112-122.
8. Neese, F., *ORCA, an ab initio, Density Functional and Semiempirical program package, Version 2.9.0* **2004**, Max-Planck-Insitut für Bioanorganische Chemie: Mülheim and der Ruhr.
9. Ernzerhof, M.; Scuseria, G. E., *J. Chem. Phys.* **1999,** *110*, 5029-5036; Adamo, C.; Barone, V., *J. Chem. Phys.* **1999,** *110*, 6158-6170; Adamo, C.; Cossi, M.; Barone, V., *THEOCHEM* **1999,** *493*, 145-157.
10. Schäfer, A.; Huber, C.; Ahlrichs, R., *J. Chem. Phys.* **1994,** *100*, 5829-5835.
11. Lenthe, E. v.; Baerends, E. J.; Snijders, J. G., *J. Chem. Phys.* **1993,** *99*, 4597-4610; van Lenthe, E.; Snijders, J. G.; Baerends, E. J., *J. Chem. Phys.* **1996,** *105*, 6505-6516; Schreckenbach, G.; Ziegler, T., *J. Phys. Chem.* **1995,** *99*, 606-611; Schreckenbach, G.; Ziegler, T., *Int. J. Quantum Chem.* **1997,** *61*, 899-918; Wolff, S. K.; Ziegler, T., *J. Chem. Phys.* **1998,** *109*, 895-905; Wolff, S. K.; Ziegler, T.; van Lenthe, E.; Baerends, E. J., *J. Chem. Phys.* **1999,** *110*, 7689-7698; Krykunov, M.; Ziegler, T.; Lenthe, E. v., *Int. J. Quantum Chem.* **2009,** *109*, 1676-1683.
12. Klamt, A.; Schuurmann, G., *J. Chem. Soc., Perkin Trans. 2* **1993**, 799-805.
13. te Velde, G.; Bickelhaupt, F. M.; Baerends, E. J.; Fonseca Guerra, C.; van Gisbergen, S. J. A.; Snijders, J. G.; Ziegler, T., *J. Comput. Chem.* **2001,** *22*, 931-967; Fonseca Guerra, C.; Snijders, J. G.; te Velde, G.; Baerends, E. J., *Theor. Chem. Acc.* **1998,** *99*, 391-403; Baerends, E. J.; Ziegler, T.; Autschbach, J.; Bashford, D.; Bérces, A.; Bickelhaupt, F. M.; Bo, C.; Boerrigter, P. M.; Cavallo, L.; Chong, D. P.; Deng, L.; Dickson, R. M.; Ellis, D. E.; van Faassen, M.; Fan, L.; Fischer, T. H.; Fonseca Guerra, C.; Franchini, M.; Ghysels, A.; Giammona, A.; van Gisbergen, S. J. A.; Götz, A. W.; Groeneveld, J. A.; Gritsenko, O. V.; Grüning, M.; Gusarov, S.; Harris, F. E.; van den Hoek, P.; Jacob, C. R.; Jacobsen, H.; Jensen, L.; Kaminski, J. W.; van Kessel, G.; Kootstra, F.; Kovalenko, A.; Krykunov, M. V.; van Lenthe, E.; McCormack, D. A.; Michalak, A.; Mitoraj, M.; Morton, S. M.; Neugebauer, J.; Nicu, V. P.; Noodleman, L.; Osinga, V. P.; Patchkovskii, S.; Pavanello, M.; Philipsen, P. H. T.; Post, D.; Pye, C. C.; Ravenek, W.; Rodríguez, J. I.; Ros, P.; Schipper, P. R. T.; Schreckenbach, G.; Seldenthuis, J. S.; Seth, M.; Snijders, J. G.; Solà, M.; Swart, M.; Swerhone, D.; te Velde, G.; Vernooijs, P.; Versluis, L.; Visscher, L.; Visser, O.; Wang, F.; Wesolowski, T. A.; van Wezenbeek, E. M.; Wiesenekker, G.; Wolff, S. K.; Woo, T. K.; Yakovlev, A. L., *ADF2013, SCM*, Theoretical Chemistry, Vrije Universiteit, Amsterdam, The Netherlands, http://www.scm.com.
14. Van Lenthe, E.; Baerends, E. J., *J. Comput. Chem.* **2003,** *24*, 1142-1156.